Uncertainty From Choice of Mode-Stirring Technique in Reverberation-Chamber Measurements

Kate A. Remley, *Fellow, IEEE*, Ryan J. Pirkl, *Member, IEEE*, Haider A. Shah, and Chih-Ming Wang

***Abstract*—We develop methods for assessing the component of measurement uncertainty arising from various combinations of mode-stirring techniques in reverberation-chamber measurements. We first develop a components-of-variance model that describes this component of uncertainty in terms of physical mechanisms related to the chamber. We illustrate the use of the model in conjunction with measurements to identify the optimal mode-stirring sequence for a measurement of received power.**

***Index Terms*—Electromagnetic measurements, measurement uncertainty, reverberation chamber, wireless communication.**

I. Introduction

IT is well known that the number of measurements and the choice of mode-stirring techniques may affect the uncertainty in reverberation-chamber measurements [1], [2]. By use of an optimal combination of stirring methods, users can significantly reduce their total measurement uncertainty, while maximizing the efficiency in their wireless-device test procedures. We illustrate this with empirical calculations of uncertainty as well as a model to identify the effects of various physical mechanisms on the observed uncertainty. An example provides users a method to characterize their own reverberation chambers to maximize efficiency and minimize uncertainty in wireless-device test.

Quantities of interest that have been studied for wireless testing in the reverberation chamber include total radiated power, total isotropic sensitivity, bit error rate, and other wireless device metrics [3]–[6]. Study of antenna parameters is common as well [7]–[9]. The fields within the chamber can be manipulated through the use of radio-frequency absorber to replicate various real-world environments, exposing a wireless device to desired conditions [10]–[13]. Reverberation chambers may be used in over-the-air test of multiple antenna systems [14], [15]. The methods discussed in this paper can be used to assess the uncertainty due to choice of mode-stirring technique in an estimate of any of these quantities of interest. We focus on the application of the methods to measurements of radiated power for illustrative purposes. Even though we focus on average received power measurements, the method may be applied to other measured quantities such as peak power, as considered in the IEC 61000-4-21 standard [16].

Ideally, for high-Q chambers exhibiting good field uniformity in an ensemble of measurements, various types of mode stirring will provide equivalent results and uncertainties [1], [2]. In practice, several factors will increase the uncertainty in the estimate of a measured quantity. For example, chamber loading decreases the Q of the chamber, increasing the relative amount of unstirred energy and increasing the correlation between measurement samples [17].

The effects on uncertainty in the estimate of a quantity of interest introduced by correlation between measurements and/or unstirred energy in the chamber are difficult to predict because they depend on chamber characteristics for each specific measurement setup, including chamber Q (and the related coherence bandwidth), chamber size, the location and size of mode-stirring paddles, and the type and orientation of the antennas.

The many complicated interactions between the chamber, the test setup, and the device or antenna under test motivate the need for empirical methods to predict uncertainty and optimize stirring for a given configuration. From knowledge of the physical mechanisms in a reverberation chamber that impact the effectiveness of mode stirring, we develop a simplified model for uncertainty. The parameters of this model may be extracted with a straightforward set of measurements. The model allows users to optimize mode-stirring sequences for a given test setup and facilitates improved measurement configurations.

In Section II, we provide a method for calculating the component of uncertainty in reverberation-chamber measurements arising from the choice of mode-stirring techniques. In Section III, we derive a components-of-variance model that relates observed changes in uncertainty to physical characteristics of the reverberation-chamber setup, such as correlation between samples and nonnegligible unstirred energy. In Section IV, we illustrate how the measurement procedure used to populate the model may also be applied directly to assess a given reverberation-chamber setup. Good agreement between modeled and measured uncertainties serves to verify the model. When combined with the model, the characterization method of Section IV can also be used to design measurement scenarios that achieve a specified level of uncertainty. In Section V, we offer some concluding remarks.

Manuscript received August 9, 2012; revised December 19, 2012; accepted January 20, 2013.

K. A. Remley and C.-M. Wang are with the National Institute of Standards and Technology, Boulder, CO 80305 USA (e-mail: kate.remley@nist.gov; chih-ming.wang@nist.gov).

R. J. Pirkl was with the National Institute of Standards and Technology, Boulder, CO 80305 USA. He is now with AT&T Mobility, Austin, TX 78759 USA (e-mail: rpirkl@gmail.com).

H. A. Shah was with the National Institute of Standards and Technology, Boulder, CO 80305 USA. He is now with Ericsson AB, Stockholm, Södermanland, Sweden (e-mail: hyder.a.shah@gmail.com).

Color versions of one or more of the figures in this paper are available online at http://ieeexplore.ieee.org.

Digital Object Identifier 10.1109/TEMC.2013.2246570

II. Effect of Mode Stirring on Measurement Uncertainty

A. Calculation of Uncertainty

When reverberation chambers are used for free-field testing of wireless devices, the measured quantity of interest is typically derived from an ensemble of measurements. The statistics of the multiple measurements may be used to estimate, with some level of uncertainty, the quantity of interest. In [18], this uncertainty was calculated for nine sets of data acquired with a specific combination of mode-stirring methods. Here, we present a generalization and extension of the empirical uncertainty characterization procedures reported in [18].

We may empirically calculate the component of uncertainty due to choice of mode-stirring method for a given chamber setup from the standard deviation in a set of T estimates, or "samples." Each sample, formed from unique measurements that utilize the same combination of stirring techniques, provides an estimate of a quantity of interest, such as radiated power. Drawing from statistically similar sets of samples allows us to assess separately the effects on measurement uncertainty of correlation for various mode-stirring techniques, as well as the effects from the unstirred energy in the chamber, among other measurement nonidealities.

For instance, to find the uncertainty in a received-power measurement utilizing a combination of M values of mode-stirring technique 1 and N values of mode-stirring technique 2, we collect T samples of $M \times N$ measurements. We then form T ensemble averages by randomly selecting measurements made with M values of technique 1 and N values of technique 2 from the entire set of $T \times M \times N$ measurements. The tth sample is given by

$$\langle P \rangle_{M,N}^{(t)} = \frac{1}{MN} \sum_{n=1}^{N} \sum_{m=1}^{M} P\left(a_m, b_n\right) \tag{1}$$

where $P\left(a_m, b_n\right)$ denotes an implicitly frequency-dependent power measurement depending on mode-stirring techniques a and b. As an example, for a measurement sequence composed of $M = 10$ antenna locations and $N = 10$ mode-stirring-paddle positions, we would conduct 100 unique measurement sequences to compute $T = 100$ unique samples $P_{10,10}^{(t)}$.

Each sample should be a representative of the proposed measurement procedure (e.g., $M \times N$ measurements for an estimate of radiated power), and all of the $T \times M \times N$ measurements should be unique. This eliminates potential bias from the use of repeat measurements or from measurements having different statistical distributions and/or correlation values than that of the proposed measurement sequence. This random selection of the measurements that form a sample would be highly unusual in practice (for example, in this characterization procedure, to form a sample, one typically selects nonadjacent paddle positions and antenna locations). However, such a technique is necessary to completely characterize a particular chamber configuration for subsequent measurements that use the same configuration.

The estimated received power will be the difference between the measured received power $\langle P \rangle_{M,N}^{(t)}$ and the noise contribution $\hat{\bar{P}}_{\text{noise}}$:

$$\hat{\bar{P}}_{\text{received}}^{(t)} = \langle P \rangle_{M,N}^{(t)} - \hat{\bar{P}}_{\text{noise}}. \tag{2}$$

Assuming the noise is additive (e.g., additive white Gaussian noise), the noise contribution may be accurately estimated from the average of Q repeat measurements of the receiver's noise floor

$$\hat{\bar{P}}_{\text{noise}} = \frac{1}{Q} \sum_{q=1}^{Q} P_{\text{noise}}. \tag{3}$$

The standard deviation of the T samples provides an estimate of the component of uncertainty in the measured power arising from a given combination of mode-stirring techniques as

$$\hat{u}_{\text{measured}} = \sqrt{\frac{1}{T-1} \sum_{t=1}^{T} \left[\langle P \rangle_{M,N}^{(t)} - \frac{1}{T} \sum_{t=1}^{T} \langle P \rangle_{M,N}^{(t)} \right]^2}. \tag{4}$$

For the estimate of received power, the additional uncertainty $\hat{u}_{\text{noise}}$ due to the noise power estimate must be included. Assuming uncorrelated noise measurements, the uncertainty in the noise power estimate is given by the standard deviation of the measurements divided by $\sqrt{Q}$:

$$\hat{u}_{\text{noise}} = \frac{1}{\sqrt{Q}} \sqrt{\frac{1}{Q-1} \sum_{q=1}^{Q} \left[P_{\text{noise}} - \hat{\bar{P}}_{\text{noise}} \right]^2}. \tag{5}$$

The combined uncertainty $\hat{u}_c$ is the root-sum-of-squares of the measurement and noise uncertainty components:

$$\hat{u}_c = \sqrt{\hat{u}_{\text{measured}}^2 + \hat{u}_{\text{noise}}^2}. \tag{6}$$

Equations (1)–(6) summarize our empirical calculation of these components of uncertainty in a received-power measurement. In order to study the relative impact of various combinations of mode-stirring techniques on measurement uncertainty, we will utilize a normalized form of uncertainty $\hat{\tilde{u}}$ given by

$$\hat{\tilde{u}}_c = \frac{\hat{u}_c}{\frac{1}{T} \sum_{t=1}^{T} \langle P \rangle_{M,N}^{(t)} - \hat{\bar{P}}_{\text{noise}}} \tag{7}$$

where we divide the combined uncertainty in a single mean received-power sample $\langle P \rangle_{M,N}^{(t)}$ by the best available estimate of the average received power based on all samples. This relative uncertainty facilitates comparisons of our measured results to those that would be expected for an ideal measurement procedure in an ideal reverberation chamber [19]; that is, one with perfect mode stirring (no unstirred energy), no correlation between measurements, and no measurement noise. The uncertainty due to mode stirring in this ideal chamber is [20]

$$\tilde{u}_{\text{ind}} = \frac{1}{\sqrt{MN}}. \tag{8}$$

Equation (8) provides a theoretical lower bound on the uncertainty in the tth sample $\hat{\bar{P}}_{\text{received}}^{(t)}$ under the assumption that the power measurements are identically exponentially distributed

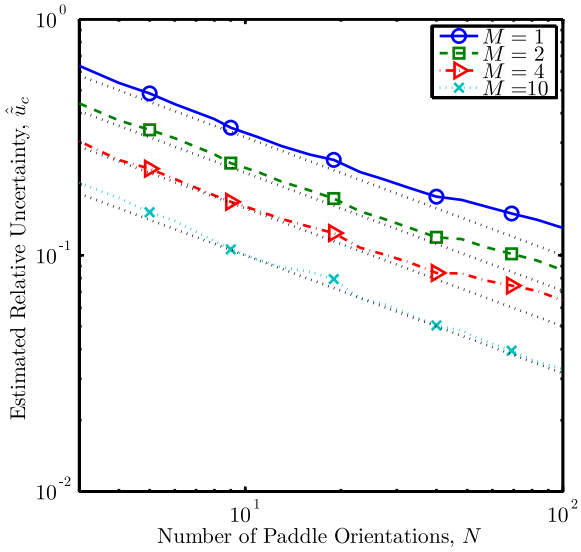

Fig. 1. Relative (normalized) uncertainty for reverberation-chamber measurements of received power for an increasing number of N paddle angles for various values of M antenna locations. The symbols represent every 20th data point. The dotted lines without symbols represent the ideal $1/\sqrt{MN}$ dependence given in (8).

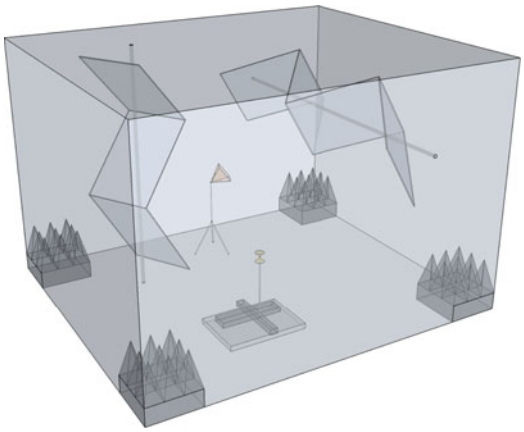

Fig. 2. Three-dimensional view of the reverberation-chamber setup used in the example above.

or, equivalently, that electric field may be described by a zero-mean complex Gaussian distributed process.[1] These assumptions are well accepted in the literature [1], [21]–[23]. Because the uncertainty is derived from a collection of multiple samples, it can be described with Type A statistical methods [19].

Fig. 1 shows the calculated relative uncertainty for measurements made in a NIST reverberation chamber involving various fixed numbers of M antenna locations and N paddle angles, respectively. A sketch of the chamber is shown in Fig. 2 and the measurement parameters are described in Table I. Note that, for convenience, we have defined the combined mode stirring of

[1]Strictly speaking, the estimated quantity of interest in [20] was the variance of the real (or imaginary) field components in a reverberation chamber. However, this quantity is directly proportional to average received power and is estimated from the mean-squared field components (which are again proportional to power), and each field component's amplitude is Rayleigh distributed. Thereby, the power in a single field component, and ultimately, the power received by an antenna (see [29]) is exponentially distributed, whereby (8) is applicable.

TABLE I
MEASUREMENT CONFIGURATION FOR THE RESULTS PRESENTED IN FIG. 1

Quantity	Value
Chamber specifications	
Interior dimensions	3.60 m x 4.27 m x 2.90 m
Paddle dimensions (cylindrical height x radius to tip of paddle)	Vertical Paddle: 2.55 m x 38.5 cm Horizontal Paddle: 3.35 m x 38.5 cm
Transmit antenna	Type: dual-ridge guide horn Bandwidth: 1-18 GHz Height: 1.0 m (approx.) Aimed toward paddle
Receive antenna	Type: Biconical (omnidirectional) Bandwidth: 1-6 GHz Height: 1.67 m
Chamber configuration	
RF absorber (loading)	4 pieces: 55 cm tall, 60 cm wide Chamber Q: ~3000 (from [1])
Paddle positions	100 (7° steps and 13° steps)
Antenna positioner	Type: Planar (rectangular movement) Number of positions: 100 (10 x 10) Spatial increment: 0.05 m
VNA measurement parameters	
Center frequency	4.5 GHz (λ = 0.067 m)
Bandwidth	100 MHz (128 points)
IF bandwidth	100 kHz
Frequency averaging	20 MHz
Reference planes	Coaxial N-type connector at antenna input ports

the paddle rotating along a horizontal axis ("Horizontal Paddle") with that from the vertically oriented "Vertical Paddle." These contributions may also be considered separately, as discussed in [17].

Measurements were conducted with a vector network analyzer (VNA). The quantity $|S_{21}|^2$ may be interpreted as a power measurement P after a suitable calibration step. Thereby, we define $\langle P\rangle_{M,N}^{(t)} = \langle |S_{21}|^2\rangle_{M,N}^{(t)}$, and $\hat{\bar{P}}_{\text{noise}}$ corresponds to an estimate of the noise floor of the VNA. In Fig. 1, frequency averaging was conducted over a bandwidth representative of a typical wireless device, as would be done in practice (see Table I). From prior measurements, we knew that both of the antennas used were well matched at these frequencies, with an S_{11} lower than -10 dB, so no mismatch correction was performed. Each curve plots $T = 10\,000/(M \times N)$ samples and the noise power was estimated from 1000 repeat noise measurements. The complete set of 10 000 measurements took approximately 10 h.

As expected, Fig. 1 shows that increasing the number of mode-stirred measurements has the effect of reducing the relative uncertainty in the estimate of received power. This is because the increased number of measurements used to estimate the mean value reduces the uncertainty in the mean, as given in (8).

As shown in Fig. 1, this component of uncertainty follows the theoretical dependence on $1/\sqrt{MN}$ for smaller numbers of mode-stirred measurements, shown by the dotted lines without symbols in the figure. However, for large numbers of

measurements, the curves deviate from theoretical values, indicating that nonideal effects reduce the effectiveness of the mode stirring. Such nonidealities include a significant unstirred energy and nonzero correlation between measurements made at various antenna locations and paddle angles.

As discussed in the next section, a model of this nonideal behavior may be used to characterize a given reverberation-chamber setup. For example, the curves shown in Fig. 1 illustrate that a combination of mode-stirring methods would be more effective for reducing uncertainty than simply increasing the number of measurements for a single stirring method. The model developed in Section III may be used to quantify this effect, as well as to determine the required number of mode-stirred measurements needed to achieve a given level of uncertainty for a specific chamber setup.

III. Modeling the Uncertainty in Reverberation-Chamber Measurements

A. Components-of-Variance Model

A components-of-variance model [24] describes measurement uncertainty in terms of the measured variance introduced by independent physical effects. This allows the user to understand the effects on uncertainty due to various physical mechanisms, including the use of different mode-stirring techniques. Without loss of generality, our discussion will again focus on paddle-angle and antenna-location stirring in the example of a received-power measurement. Other mode-stirring techniques may be assessed with this type of model as well. The model relates the covariances between pairs of measurements to the covariances of the contributing individual physical mechanisms under a set of simplifying assumptions, as described below.

To develop the model, we first define the complex transfer function for an individual measurement as $S_{21}(r_m, \theta_n)$, where r_m and θ_n denote the antenna location and paddle angle, respectively. We again suppress the frequency dependence of $S_{21}(r_m, \theta_n)$. As mentioned previously, frequency may also be included as a separate stirring mechanism. However, for wireless test, the frequency band of operation is typically fixed, and thus, we will always present results that are averaged over the frequency band of interest. We implement the components-of-variance model by representing $S_{21}(r_m, \theta_n)$ as a superposition of three independent stochastic processes, each corresponding to a different physical process in the reverberation chamber. For our case, we have

$$S_{21}(r_m, \theta_n) = S_{21}^u(r_m) + S_{21}^s(r_m, \theta_n) + S_{21}^\varepsilon(r_m, \theta_n). \tag{9}$$

The purely spatially dependent term, $S_{21}^u(r_m)$, corresponds to the complex summation of multipath components that have not interacted with the paddle and, by definition, is independent of the orientation of the paddles. $S_{21}^u(r_m)$ is often referred to as the unstirred component of the reverberation chamber's wireless channel [1]. The mean in this quantity tends toward zero for increasing numbers of antenna locations [25].

The second term, $S_{21}^s(r_m, \theta_n)$, corresponds to the complex summation of multipath components that have been randomized either through interactions with the reverberation chamber's mode-stirring paddles or by some other mechanism such as movement of the receive antenna within the chamber. This component, which is commonly referred to as the chamber's stirred wireless channel contribution, describes a wireless channel that varies as a function of both antenna location and paddle angle [1].

The final term, $S_{21}^\varepsilon(r_m, \theta_n)$, describes contributions to the complex channel response due to measurement repeatability including noise, operator error, and calibration errors, among others. This contribution is randomly varying for all antenna locations r_m and paddle angles θ_n. We shall model each of the terms of (9) as zero-mean, complex circular, and Gaussian distributed stochastic processes. This statistical model is commonly assumed for the stirred component of S_{21}, as well as noise. We assume a similar model may be used to describe the spatial variations of the unstirred component $S_{21}^u(r_m)$. Further justification and detail of the assumed distributions are presented in Appendix A.

B. Modeling the Uncertainty in Average Received Power

Similar to (1), the received power is estimated from an ensemble average of VNA measurements

$$\hat{\bar{P}}_{\text{measured}} = \frac{1}{MN}\sum_{m=1}^{M}\sum_{n=1}^{\text{N}} |S_{21}(r_m, \theta_n)|^2 \tag{10}$$

with the understanding that a power-meter calibration would be necessary to find the true power.

The received power is given by the difference between $\hat{\bar{P}}_{\text{measured}}$ and a noise power estimate $\hat{\bar{P}}_{\text{noise}}$, as given in (2). The combined uncertainty $\hat{u}_c$ is given by $\hat{u}_{\text{measured}}$ and the estimated noise power $\hat{u}_{\text{noise}}$, as given in (6).

The uncertainty in $\hat{\bar{P}}_{\text{measured}}$ may be determined from its variance, denoted $\sigma^2_{\hat{\bar{P}}_{\text{measured}}}$, which is equal to the average of the covariances between all measurements of $|S_{21}(r_m, \theta_n)|^2$ [24]. By use of Appendix A [see (A1)–(A8)], we may express $\sigma^2_{\hat{\bar{P}}_{\text{measured}}}$ as

$$\begin{aligned}\sigma^2_{\hat{\bar{P}}_{\text{measured}}} &= \frac{1}{MN}\left[P^u + P^s + P^\varepsilon\right]^2 \\ &\quad + \rho_r^2\frac{M-1}{MN}\left[P^u + P^s\right]^2 + \frac{N-1}{MN}\left[P^u + P^s\rho_\theta\right]^2 \\ &\quad + \rho_r^2\frac{(M-1)(N-1)}{MN}\left[P^u + P^s\rho_\theta\right]^2. \end{aligned}\tag{11}$$

We define the noise power estimate over q mode-stirred measurements as

$$\hat{\bar{P}}_{\text{noise}} = \frac{1}{Q}\sum_{q=1}^{\text{Q}} |S_{21}^\varepsilon(r_q, \theta_q, q)|^2 \tag{12}$$

whereby $\hat{\bar{P}}_{\text{noise}}$ is determined from an auxiliary noise power measurement, and the variance in the noise power estimate is

$$\sigma^2_{\hat{\bar{P}}_{\text{noise}}} = \left\{\frac{1}{Q}\left[P^\varepsilon\right]^2\right\}. \tag{13}$$

As in Section II, it is often more convenient to express the uncertainty in a normalized form whereby we divide $u_{\rm tot}$ by the mean received power, as given by the sum of the unstirred and stirred components' powers. Thus, the relative uncertainty $\tilde{u}_c$ is

$$\tilde{u}_c = \frac{u_c}{P^u + P^s} \tag{14}$$

which is the analog to the estimated relative uncertainty $\hat{\tilde{u}}_c$ presented in (7). From (14), we find that the theoretical relative uncertainty is given by

$$\begin{aligned}\tilde{u}_c = \frac{1}{P^u + P^s} \Bigg\{ & \frac{1}{MN} \left[P^u + P^s + P^\varepsilon\right]^2 \\ & + \rho_r^2 \frac{M-1}{MN} \left[P^u + P^s\right]^2 + \frac{N-1}{MN} \left[P^u + P^s \rho_\theta\right]^2 \\ & + \rho_r^2 \frac{(M-1)(N-1)}{MN} \left[P^u + P^s \rho_\theta\right]^2 + \frac{1}{Q} \left[P^\varepsilon\right]^2 \Bigg\}^{\frac{1}{2}}.\end{aligned} \tag{15}$$

To clearly assess the effects of various mode-stirring methods on measurement uncertainty, we will next rewrite (15) in terms of a spatially averaged Rician K-factor K, defined as the ratio of unstirred power to stirred power [11]:

$$K = \frac{P^u}{P^s}. \tag{16}$$

A low *K*-factor ($K \ll 1$) is generally desirable because fewer measurements are required to obtain sufficiently randomized measured fields with a given level of uncertainty. With (16), (15) becomes

$$\begin{aligned}\tilde{u}_c = \frac{1}{K+1} \Bigg\{ & \frac{1}{MN} \left[K + 1 + \frac{P^\varepsilon}{P^s}\right]^2 + \rho_r^2 \frac{M-1}{MN} [K+1]^2 \\ & + \frac{N-1}{MN} \left[K + \rho_\theta\right]^2 + \rho_r^2 \frac{(M-1)(N-1)}{MN} \left[K + \rho_\theta\right]^2 \\ & + \frac{1}{Q} \left[\frac{P^\varepsilon}{P^s}\right]^2 \Bigg\}^{\frac{1}{2}}.\end{aligned} \tag{17}$$

The physical contributions to uncertainty from paddle-angle and antenna-position uncertainty may be understood by considering (17) for the cases of a single antenna location with multiple paddle angles (i.e., $M = 1$ and $N \gg 1$), and for a single paddle angle with multiple antenna locations (i.e., $N = 1$ and $M \gg 1$). Neglecting measurement noise, we have

$$\tilde{u}_c|_{M=1} = \sqrt{\frac{1}{N} + \frac{N-1}{N} \left[\frac{K + \rho_\theta}{K+1}\right]^2} \tag{18}$$

and

$$\tilde{u}_c|_{N=1} = \sqrt{\frac{1}{M} + \rho_r^2 \frac{M-1}{M}}. \tag{19}$$

We see that for a single antenna location ($M = 1$), the uncertainty will be dominated by the sum of the Rician K-factor and the paddle-angle correlation ρ_θ, whereas for a single paddle angle ($N = 1$), the uncertainty will be dominated by the antenna-location correlation ρ_r. Equation (17) indicates that it is possible to find an optimal measurement sequence to minimize uncertainty in the presence of the nonidealities of K, ρ_θ, and ρ_r.

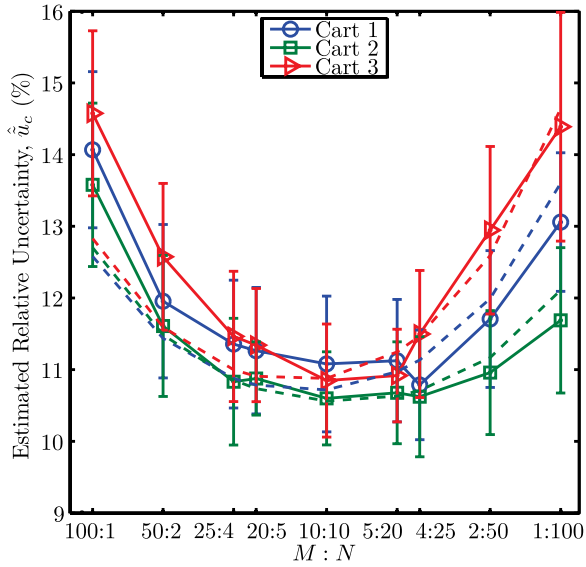

Fig. 3. Ratio of the number of M antenna locations to the number of N paddle angles for $T = 100$ samples of $MN = 100$ reverberation-chamber measurements. Solid lines: Measured results. Dashed lines: Results for the components-of-variance model presented in Section III. The error bars represent the standard deviation in the uncertainty over a 20 MHz frequency band and the markers denote cart locations illustrated in Fig. 4.

IV. Model Verification and Measurement Technique

We next present a measurement-based method for identifying the optimal mode-stirring sequence for a given reverberation-chamber setup. We verify the above simplified model by estimating its parameters from measured data, illustrating agreement with measurements for a variety of mode-stirring configurations. Once the model parameters have been estimated, the model can then be used for experiment design in future measurements.

To illustrate the technique, we again find the uncertainty in a received-power measurement made in a reverberation chamber with a mode-stirring sequence for combinations of M antenna locations and N paddle angles for $MN = 100$. By use of (1), we calculate T samples from S-parameter measurements, where the tth sample is given by

$$\left\langle |S_{21}|^2 \right\rangle_{M,N}^{(t)} = \frac{1}{MN} \sum_{n=1}^{N} \sum_{m=1}^{M} |S_{21}(r_m, \theta_n)|^2. \tag{20}$$

Here, $S_{21}(r_m, \theta_n)$ denotes a measurement at antenna location r_m and paddle angle θ_n. Frequency dependence is again suppressed.

For the example here, we conducted a set of 10 000 $|S_{21}|^2$ measurements from which we were able to compute $T = 100$ unique samples $\left\langle |S_{21}|^2 \right\rangle_{M,N}^{(t)}$ satisfying $MN = 100$. An estimate of the noise power was obtained from 1000 repeat measurements by use of (3), and the relative combined uncertainty was estimated by use of (4)–(7).

Fig. 3 shows the relative uncertainty estimate derived from measurement, as defined in (6), for various combinations of

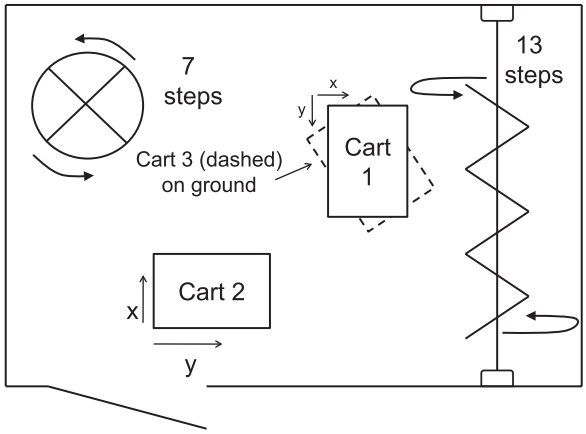

Fig. 4. Antenna-positioner cart locations within the reverberation chamber for the measurement data presented in Fig. 3. The antenna positioner was used to assess uncertainty over a local area within the chamber, while the cart locations provided uncertainty at different large-scale locations within the chamber.

TABLE II
PARAMETER ESTIMATION RESULTS FOR CART LOCATIONS 1–3

Parameter	Cart Location	Estimate
$\hat{\rho}_r$	1	0.08
	2	0.08
	3	0.08
$\hat{\rho}_\theta$	1	0.02
	2	0.02
	3	0.02
$\widehat{K}$	1	0.10
	2	0.07
	3	0.12
$\hat{P}^\epsilon/\hat{P}^s$	1	0.01
	2	0.01
	2	0.01

M antenna locations and N paddle angles for the $T = 100$ samples. The different curves correspond to different antenna-positioner locations within the chamber, each separated from the other by large-scale, multiple-wavelength distances, as shown in Fig. 4. The measurement configuration for these graphs is again described in Table I with one exception: when the antenna positioner was placed on the floor of the chamber (denoted Cart 3), the height of the receive antenna was 90 cm rather than 1.67 m as for the other two cart locations. The error bars correspond to a ± 1 standard deviation in the estimated relative uncertainty.

Estimates of ρ_r, ρ_θ, K, and $\hat{P}^\varepsilon/\hat{P}^s$ for the relative uncertainty model of (17) were extracted from the measurement data. The antenna-location and paddle-angle correlation coefficients, $\hat{\rho}_r$ and $\hat{\rho}_\theta$, were estimated as the root-mean-square correlation between all pairs of antenna locations and paddle angles, respectively. For example, for $\hat{\rho}_r$, we estimated the correlation between measurements for different pairs of antenna locations. We then calculated the root mean square of this set of correlation coefficients, which we used as our estimate of $\hat{\rho}_r$.

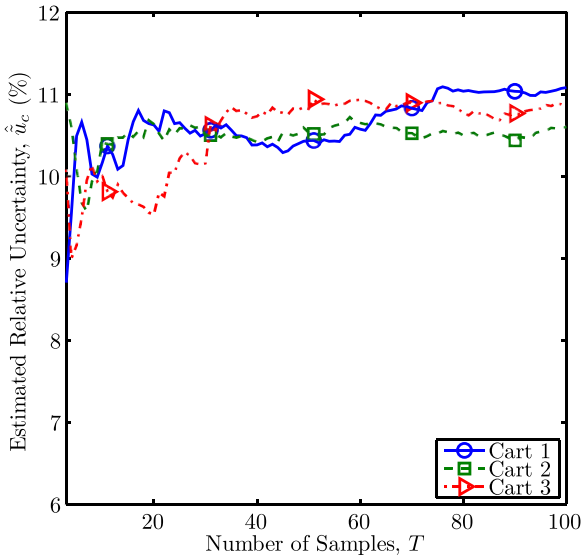

Fig. 5. Estimated relative uncertainty for different numbers of samples T for $M = 10$ antenna locations and $N = 10$ paddle orientations.

Table II provides the model parameters based on our measurements. The set of parameters indicates that the antenna-location correlations and Rician K-factors are large when compared to the paddle-angle correlations and normalized measurement noise.

The dashed line in Fig. 3 represents the results from the relative uncertainty model of (17). With the exception of one sample point, the modeled curves fall within the error bars of the measured curves, verifying that the simplified components-of-variance model of (17) adequately captures the key physical mechanisms within the reverberation chamber.

Fig. 3 provides an easy way to identify the optimal mode-stirring sequence for various reverberation-chamber configurations. For this example, no matter which cart location is used, the ratio of approximately $M = 10$ antenna locations to $N = 10$ paddle angles clearly minimizes the component of uncertainty due to mode stirring. The equal ratio of ten antenna locations and ten paddle angles indicates that these two stirring mechanisms provide similar levels of mode stirring for this particular chamber setup. If the performance of one stirring mechanism is different from another, the ratio will change. Fig. 3 indicates that a poor choice of stirring methods and/or sequences may lead to increased correlation between measurements and thereby increased measurement uncertainty. Similar findings were reported in [26].

For the measured results shown here, we see from (18) and (19) that an increase in uncertainty can be attributed to spatial correlation between measurements when antenna-location stirring was used, and to the effects of the nonzero Rician K-factor when paddle-angle stirring was used. Further, the uncertainty arising from paddle stirring was not equivalent for all locations in the chamber, presumably due to differences in the Rician K-factor at each location.

Graphs such as those in Fig. 3 can also be used to estimate the expected increase in uncertainty if a suboptimal stirring sequence is chosen. For example, in the NIST reverberation chamber, antenna-location stirring is not convenient. We must either insert an antenna positioner into the chamber or manually move the antennas. Thus, for a given measurement, it may be desirable to accept an increase in the estimated uncertainty in order to utilize a less time-consuming stirring sequence.

In practice, it may not be necessary to collect 100 samples (corresponding to 10 000 measurements) in order to assess the component of uncertainty due to mode stirring. In Fig. 5, we illustrate the change in the estimated uncertainty when we reduce the number of samples T used in the uncertainty calculation in (6). Taking the estimated relative uncertainty for $T = 100$ as the true value, we see that the uncertainty estimate is within 0.5% when $T > 20$ samples are used.

The method presented here for identifying optimal stirring sequences shows that, for large chambers such as the one studied here, location effects on both a local scale (on the order of a wavelength), represented here by the within-cart variation, and large-scale effects within the chamber, represented here by the cart-to-cart variation, must be considered. In conjunction with measurement data, the model of (17) may be used to determine what underlying factors affect the measurement uncertainty for each reverberation-chamber measurement configuration.

V. Summary and Conclusion

We have presented modeling and measurement techniques that allow reverberation-chamber users to assess the significant and measurable effect on uncertainty of mode-stirring technique and number of measurements. Our model describes the component of measurement uncertainty related to mode stirring in terms of the variance arising from independent physical effects in the reverberation chamber. The measurement technique may be used to assess this component of uncertainty empirically. This component of uncertainty may be combined with other sources of measurement uncertainty to provide a complete error analysis, a goal of future work.

It should be possible to use the modeling technique presented here to study the uncertainty arising from measurements made with reverberation chambers that are only slightly oversized. Models are typically used in such cases due to the difficulty of generating independent spatial and stirrer positions.

By use of the measurement and modeling techniques described here, users may assess the source of uncertainty due to mode stirring. These techniques can be utilized directly to design appropriate stirring sequences and to reduce uncertainties in measurements and/or design experiments to achieve a desired level of uncertainty.

Appendix A

Statistical Model for S_{21} Measurements in a Reverberation Chamber

We assume that each of the terms in (9) may be modeled by independent, complex, circular, and zero-mean Gaussian distributions:

$$S_{21}^{u}\left(r_m\right) \sim \mathcal{N}\left(0,\sigma_u^2\right) + j\mathcal{N}(0,\sigma_u^2) \tag{A1}$$

$$S_{21}^{s}\left(r_m,\theta_n\right) \sim \mathcal{N}\left(0,\sigma_s^2\right) + j\mathcal{N}(0,\sigma_s^2) \tag{A2}$$

$$S_{21}^{\varepsilon}\left(r_m,\theta_n,l\right) \sim \mathcal{N}\left(0,\sigma_\varepsilon^2\right) + j\mathcal{N}(0,\sigma_\varepsilon^2) \tag{A3}$$

where $\mathcal{N}\left(\mu,\sigma^2\right)$ represents a Gaussian distribution having a mean μ, and a variance σ^2. Hill [1] has established that (A2) may be used to represent the stirred fields in a reverberation chamber, and (A3) is commonly used to describe noise. As was shown in [27], the unstirred fields may be composed of a large number of multipath components. Provided that these multipath components have comparable amplitudes and uncorrelated phases, the central-limit theorem dictates that the observed field will tend toward a zero-mean complex Gaussian distribution [28]. This supports our assumed model for $S_{21}^{u}\left(r_m\right)$ given in (A1).

The average power due to each term in (9) may be given by the sum of the variances of its real and imaginary components [11]:

$$P^u = \left\langle \left|S_{21}^{u}\left(r_m\right)\right|^2 \right\rangle_M = 2\sigma_u^2 \tag{A4}$$

$$P^s = \left\langle \left|S_{21}^{s}\left(r_m,\theta_n\right)\right|^2 \right\rangle_M = \left\langle \left|S_{21}^{s}\left(r_m,\theta_n\right)\right|^2 \right\rangle_N = 2\sigma_s^2 \tag{A5}$$

$$\begin{aligned} P^\varepsilon &= \left\langle \left|S_{21}^{\varepsilon}\left(r_m,\theta_n,l\right)\right|^2 \right\rangle_M = \left\langle \left|S_{21}^{\varepsilon}\left(r_m,\theta_n,l\right)\right|^2 \right\rangle_N \\ &= \left\langle \left|S_{21}^{\varepsilon}\left(r_m,\theta_n,l\right)\right|^2 \right\rangle_L = 2\sigma_\varepsilon^2 \end{aligned} \tag{A6}$$

where P^u, P^s, and P^ε are the unstirred, stirred, and noise power, respectively; $\langle\ \rangle_M$, $\langle\ \rangle_N$, and $\langle\ \rangle_L$ represent an ensemble average with respect to antenna locations r_m, paddle angles θ_n, and repeat measurements l, respectively. We have assumed all terms to be ergodic with respect to their dependent variables, whereby the mean and variance of each term may be estimated from a set of observations (for example, at different antenna locations r_m).

We quantify the interactions among S_{21}^u, S_{21}^s, and S_{21}^ε in terms of covariances that depend on the average powers from (A4)–(A6), as well as a set of correlations, as

$$\operatorname{cov}\left[S_{21}^{u}\left(r_m\right), S_{21}^{u}\left(r_{m'}\right)\right] = P^u \times \begin{cases} 1 & m = m' \\ \rho_r & m \neq m' \end{cases} \tag{A7}$$

$$\begin{aligned} &\operatorname{cov}\left[S_{21}^{s}\left(r_m,\theta_n\right), S_{21}^{s}\left(r_{m'},\theta_{n'}\right)\right] \\ &= P^s \times \begin{cases} 1 & m = m', n = n' \\ \rho_r & m \neq m', n = n' \\ \rho_\theta & m = m', n \neq n' \\ \rho_{r,\theta} & m \neq m', n \neq n' \end{cases} \end{aligned} \tag{A8}$$

$$\begin{aligned} &\operatorname{cov}\left[S_{21}^{\varepsilon}\left(r_m,\theta_n,l\right), S_{21}^{\varepsilon}\left(r_{m'},\theta_{n'},l'\right)\right] \\ &= P^\varepsilon \times \begin{cases} 1 & m = m', n = n', l = l' \\ 0 & \text{otherwise} \end{cases} \end{aligned} \tag{A9}$$

where ρ_r and ρ_θ denote the correlation between different antenna locations r_m and paddle angles θ_n, respectively. The term $\rho_{r,\theta}$ describes a joint correlation between two measurements at different antenna locations and paddle angles, and the primed indices correspond to (potentially) paddle angles or antenna locations different from the unprimed case. In (A7)–(A9), we have

assumed a constant correlation model, whereby we assign the same antenna-location/paddle-angle correlation between observation pairs regardless of the particular antenna location and/or paddle angle. We also assume that $\rho_{r,\theta}$ is equal to the product of the two individual correlations

$$\rho_{r,\theta} = \rho_r \rho_\theta . \tag{A10}$$

By use of (9) and (A7)–(A10), the overall covariance in a set of measurements of $S_{21}\left(r_m, \theta_n, l\right)$ is given by

$$\begin{aligned} &\operatorname{cov}\left[S_{21}\left(r_m, \theta_n, l\right), S_{21}\left(r_{m'}, \theta_{n'}, l'\right)\right] \\ &= \begin{cases} P^u + P^s + P^\varepsilon & m = m', n = n', l = l' \\ P^u + P^s & m = m', n = n', l \neq l' \\ P^u \rho_r + P^s \rho_r & m \neq m', n = n' \\ P_u^u + P^s \rho_\theta & m = m', n \neq n' \\ P^u \rho_r + P^s \rho_r \rho_\theta & m \neq m', n \neq n'. \end{cases} \end{aligned} \tag{A11}$$

REFERENCES

[1] D. Hill, *Electromagnetic Fields in Cavities: Deterministic and Statistical Theories*. Piscataway, NJ, USA: Wiley-IEEE Press, 2009.

[2] D. Hill, "Electronic mode stirring for reverberation chambers," *IEEE Trans. Electromagn. Compat.*, vol. 36, no. 4, pp. 294–299, Nov. 1994.

[3] U. Carlberg, P.-S. Kildal, A. Wolfgang, and O. Sotoudeh, "Calculated and measured absorption cross sections of lossy objects in reverberation chamber," *IEEE Trans. Electromagn. Compat.*, vol. 46, no. 2, pp. 146–154, May 2004.

[4] C. Orlenius, P.-S. Kildal, and G. Poilasne, "Measurements of total isotropic sensitivity and average fading sensitivity of CDMA phones in reverberation chamber," in *Proc. IEEE Int. Symp. Antennas Propag. Soc.*, Washington, DC, USA, Jul. 3–8, 2005, pp. 409–412.

[5] V. Monebhurrun and T. Letertre, "Total radiated power measurements of WiFi devices using a compact reverberation chamber," in *Proc. 20th Int. Zurich Symp. Electromagn. Compat.*, Jan. 12–16, 2009, pp. 65–68.

[6] S. J. Floris, K. A. Remley, and C. L. Holloway, "Bit error rate measurements in reverberation chambers using real-time vector receivers," *IEEE Antennas Wireless Propag. Lett.*, vol. 9, pp. 619–622, 2010.

[7] K. Rosengren and P.-S. Kildal, "Radiation efficiency, correlation, diversity gain and capacity of a six-monopole antenna array for a MIMO system: Theory, simulation, and measurement in reverberation chamber," *IEE Proc.—Microw. Antennas Propag.*, vol. 152, no. 1, pp. 7–16, 2005.

[8] N. Serafimov, P.-S. Kildal, and T. Bolin, "Comparison between radiation efficiencies of phone antennas and radiated power of mobile phones measured in anechoic chambers and reverberation chambers," in *Proc. IEEE Int. Symp. Antennas Propag. Soc.*, San Antonio, TX, USA, 2002, vol. 2, pp. 478–481.

[9] C. L. Holloway, H. A. Shah, R. J. Pirkl, W. Young, D. A. Hill, and J. M. Ladbury, "Reverberation chamber techniques for determining the radiation and total efficiency of antennas," *IEEE Trans. Antennas Propag.*, vol. 60, no. 4, pp. 1758–1770, Apr. 2012.

[10] M. Otterskog and K. Madsen, "On creating a nonisotropic propagation environment inside a scattered chamber," *Microw. Opt. Technol. Lett.*, vol. 43, no. 3, pp. 192–195, 2004.

[11] C. L. Holloway, D. A. Hill, J. M. Ladbury, P. F. Wilson, G. Koepke, and J. Coder, "On the use of reverberation chambers to simulate a Rician radio environment for the testing of wireless devices," *IEEE Trans. Antennas Propag.*, vol. 54, no. 11, pp. 3167–3177, Nov. 2006.

[12] X. Chen, P.-S. Kildal, C. Orlenius, and J. Carlsson, "Channel sounding of loaded reverberation chamber for over-the-air testing of wireless devices—Coherence bandwidth versus average mode bandwidth and delay spread," *IEEE Antennas Wireless Propag. Lett.*, vol. 8, pp. 678–681, 2009.

[13] H. Fielitz, K. A. Remley, C. L. Holloway, D. Matolak, Q. Zhang, and Q. Wu, "Reverberation-chamber test environment for outdoor urban wireless propagation studies," *IEEE Antennas Wireless Propag. Lett.*, vol. 9, pp. 52–56, 2010.

[14] P.-S. Kildal and K. Rosengren, "Correlation and capacity of MIMO systems and mutual coupling, radiation efficiency, and diversity gain of their antennas: Simulation and measurement in a reverberation chamber," *IEEE Commun. Mag.*, vol. 42, no. 12, pp. 104–112, Dec. 2004.

[15] J. Valenzuela-Valdés, A. Martínez-González, and D. Sánchez-Hernández, "Emulation of MIMO nonisotropic environments with reverberation chambers," *IEEE Antennas. Wireless Propag. Lett.*, vol. 7, pp. 325–328, 2008.

[16] *Electromagnetic Compatibility Part 4–21*, IEC Standard, 2003.

[17] R. J. Pirkl, K. A. Remley, and C. S. Patané, "Reverberation chamber measurement correlation," *IEEE Trans. Electromagn. Compat.*, vol. 54, no. 3, pp. 533–545, Jun. 2012.

[18] P.-S. Kildal, S.-H. Lai, and X. Chen, "Direct coupling as a residual error contribution during OTA measurements of wireless devices in reverberation chamber," in *Proc. IEEE Int. Symp. Antennas Propag. Soc.*, Charleston, SC, USA, Jun. 1–5, 2009, pp. 1–4.

[19] B. N. Taylor and C. E. Kuyatt, *Guidelines for Evaluating and Expressing the Uncertainty of NIST Measurement Results*, NIST Technical Note 1297, 1994

[20] J. G. Kostas and B. Boverie, "Statistical model for a mode-stirred chamber," *IEEE Trans. Electromagn. Compat.*, vol. 33, no. 4, pp. 366–370, Nov. 1991.

[21] P. Corona, J. Ladbury, and G. Latmiral, "Reverberation-chamber research—then and now: A review of early work and comparison with current understanding," *IEEE Trans. Electromagn. Compat.*, vol. 44, no. 1, pp. 87–94, Feb. 2002.

[22] P. Corona, G. Latmiral, E. Paolini, and L. Piccioli, "Use of a reverberating enclosure for measurements of radiated power in the microwave range," *IEEE Trans. Electromagn. Compat.*, vol. EMC-18, no. 2, pp. 54–59, May 1976.

[23] C. Lemoine, P. Besnier, and M. Drisse, "Investigations of reverberation chamber measurements through high-power goodness-of-fit tests," *IEEE Trans. Electromagn. Compat.*, vol. 49, no. 4, pp. 745–755, Nov. 2007.

[24] R. M. Mickey, O. J. Dunn, and V. A. Clark, *Applied Statistics: Analysis of Variance and Regression*, 3rd ed. Hoboken, NJ, USA: Wiley, 2004.

[25] K. Rosengren, P.-S. Kildal, C. Carlsson, and J. Carlsson, "Characterization of antennas for mobile and wireless terminals in reverberation chambers: Improved accuracy by platform stirring," *Microw. Opt. Technol. Lett.*, vol. 30, no. 6, pp. 391–397, 2001.

[26] F. Moglie, "Analysis of the independent positions of reverberation chamber stirrers as a function of their operating conditions," *IEEE Trans. Electromagn. Compat.*, vol. 53, no. 2, pp. 288–295, May 2011.

[27] R. J. Pirkl, J. M. Ladbury, and K. A. Remley, "The reverberation chamber's unstirred field: A validation of the image theory interpretation," in *Proc. IEEE Int. Symp. Electromagn. Compat.*, Long Beach, CA, USA, Aug. 14–19, 2011, pp. 670–675.

[28] R. H. Clarke, "A statistical theory of mobile-radio reception," *Bell Syst. Tech. J.*, vol. 47, no. 6, pp. 957–1000, 1968.

[29] D. A. Hill, "Plane wave integral representation for fields in reverberation chambers," *IEEE Trans. Electromagn. Compat.*, vol. 40, no. 3, pp. 209–217, Aug. 1998.

Kate A. Remley (S'92–M'99–SM'06–F'13) was born in Ann Arbor, MI, USA. She received the Ph.D. degree in electrical and computer engineering from Oregon State University, Corvallis, USA, in 1999.

From 1983 to 1992, she was a Broadcast Engineer in Eugene, OR, USA, serving as a Chief Engineer of an AM/FM broadcast station from 1989 to 1991. In 1999, she joined the Electromagnetics Division of the National Institute of Standards and Technology (NIST), Boulder, CO, USA, as an Electronics Engineer, where she is currently the Leader of the Metrology for Wireless Systems Project. Her current research interests include development of calibrated measurements for microwave and millimeter-wave wireless systems, characterizing the link between nonlinear circuits and system performance, and developing standardized test methods for RF equipment used by the public-safety community.

Dr. Remley was the recipient of the Department of Commerce Bronze and Silver Medals, the Automatic RF Techniques Group Best Paper Award. She is a member of the Oregon State University Academy of Distinguished Engineers. She was the Chair of the MTT-11 Technical Committee on Microwave Measurements from 2008 to 2010 and the Editor-in-Chief of *IEEE Microwave Magazine* from 2009 to 2011.

Ryan J. Pirkl (S'06–M'10) received the B.S., M.S., and Ph.D. degrees in electrical engineering from the Georgia Institute of Technology, Atlanta, USA, in 2005, 2007, and 2010, respectively. For the graduate research, he developed hardware, measurement procedures, and processing tools for *in situ* characterization of radio wave propagation mechanisms.

In 2010, he joined the National Institute of Standards and Technology, Boulder, CO, USA, as a National Research Council Postdoctoral Research Associate, where he investigated how reverberation chambers may be used as tunable wireless channel emulators for wireless device testing. In 2012, he joined the Subscriber Product Engineering team at AT&T Mobility, Atlanta, GA, USA. His research interests include reverberation chambers, radio wave propagation, and analytical electromagnetics.

Haider A. Shah was born in Peshawar, Pakistan, in 1985. He received the B.S. degree in electrical engineering from the COMSATS Institute of Information Technology, Islamabad, Pakistan, in 2007, and the M.S. degree in electrical engineering (telecommunication) from the Chalmers University of Technology, Gothenburg, Sweden, in 2010.

From June 2007 to July 2008, he was with Nokia Siemens Networks, as a Base Station Sub-System Engineer. He has worked as a Guest Researcher at the National Institute of Standards and Technology, Boulder, CO, USA. He is currently a Radio Performance Testing Engineer at Ericsson AB, Stockholm, Sweden. His research interest includes wireless communication and signal processing.

Chih-Ming Wang received the Ph.D. degree in statistics from Colorado State University, Fort Collins, USA, in 1978.

Since 1988, he has been with the Statistical Engineering Division, National Institute of Standards and Technology, Boulder, CO, USA. He has published more than 80 journal articles. His research interests include statistical metrology and the application of statistical methods to physical sciences.

Dr. Wang is a Fellow of the American Statistical Association (ASA). He is the recipient of the Department of Commerce Bronze Medals, the Allen V. Astin Measurement Science Award, and several awards from ASA.